

Characterizing the Strong Earth Gravity Prior

Björn Jörge^{1*} and Joan López-Moliner²

¹ Center for Vision Research, York University, 4700 Keele Street, Toronto, ON M3J 1P3, Canada

² Vision and Control of Action (VISCA) group, Department of Cognition, Development and Psychology of Education, Institut de Neurociències, Universitat de Barcelona, Ps. Vall d'Hebron 171, 08035 Barcelona, Catalonia, Spain.

* Corresponding Author

Abstract

Humans expect downwards moving objects to accelerate and upwards moving objects to decelerate. These results have been interpreted as humans maintaining an internal model of gravity. We have previously suggested an interpretation of these results within a Bayesian framework of perception: earth gravity could be represented as a Strong Prior that overrules noisy sensory information (Likelihood) and therefore attracts the final percept (Posterior) very strongly. Based on this framework, we use published data from a timing task involving gravitational motion to determine the mean and the standard deviation of the Strong Earth Gravity Prior. To get its mean, we refine a model of mean timing errors we proposed in a previous paper (Jörge & López-Moliner, 2019), while expanding the range of conditions under which it yields adequate predictions of performance. This underscores our previous conclusion that the gravity prior is likely to be very close to 9.81 m/s^2 . To obtain the standard deviation, we identify different sources of sensory and motor variability reflected in timing errors. We then model timing responses based on quantitative assumptions about these sensory and motor errors for a range of standard deviations of the

22 earth gravity prior, and find that a standard deviation of around 2 m/s² makes for the best fit. This value
23 is likely to represent an upper bound, as there are strong theoretical reasons along with supporting
24 empirical evidence for the standard deviation of the earth gravity being lower than this value.

25 Introduction

26 There is ample evidence that humans represent earth gravity and use it for a variety of tasks such as
27 interception (Ceccarelli et al., 2018; La Scaleia, Zago, Moscatelli, Lacquaniti, & Viviani, 2014; J McIntyre,
28 Zago, & Berthoz, 2001; Mijatovic, La Scaleia, Mercuri, Lacquaniti, & Zago, 2014; Senot et al., 2012; Zago
29 et al., 2004a, 2004b; Zago, La Scaleia, Miller, & Lacquaniti, 2011; Zago & Lacquaniti, 2005a; Zago, McIntyre,
30 Senot, & Lacquaniti, 2008), time estimation (Moscatelli & Lacquaniti, 2011), the perception of biological
31 motion (Maffei et al., 2015) and many more. Recently, we have shown that gravity-based prediction for
32 motion during an occlusion matched performance under a 1g expectation not only qualitatively, but also
33 quantitatively (Jörges & López-Moliner, 2019). This was an important finding to support our interpretation
34 of the above results as a strong prior in a Bayesian framework of perception (Jörges & López-Moliner,
35 2017). The results presented in (Jörges & López-Moliner, 2019) indicate that temporal errors in a timing
36 task were consistent with a mean of 1g (9.81 m/s²) when occlusions were long enough. In the present
37 paper, we extend the simulations brought forward in our previous paper: First, we consider how
38 accounting for the Aubert-Fleischl effect, which leads humans to perceive moving object at about 80% of
39 their actual speed when they pursue the target with their eyes (Aubert, 1887; Dichgans, Wist, Diener, &
40 Brandt, 1975; Fleischl, 1882), can extend our simple 1g-based model to shorter occlusions. Furthermore,
41 to fully characterize a prior, we need to not only indicate its mean, but also its standard deviation. The
42 second goal of the present paper is thus to determine the standard deviation of the strong gravity prior.
43 We aim to achieve this goal by simulations based on assumptions about the different sources of noise
44 relevant to the task at hand.

~~On a theoretical level~~In this paper, we adopt a ~~representationalistconstructivist-computational~~
~~framework~~ (Marr, 1982; Nanay, 2014); ~~we view perception as a process by which humans~~ acknowledge the
state of the world around us based on both prior knowledge and sensory online information ~~obtain~~
~~internal representations that~~ in order to guide their interactions with the external world. Please note that
~~other psychological traditions, such as ecological perception~~ (Gibson, 1986), ~~deny the necessity of~~
~~mentalprior knowledge-representations.~~ ~~we~~ Within our ~~representationalistconstructivist~~ framework, we
 envision (visual) perception as a two-step process: Encoding and Decoding (Gold & Shadlen, 2007;
 Schneidman, Bialek, & Li, 2003). During Encoding, low level signals such as luminosity, retinal velocities or
 orientation are picked up by the perceptual system and represented as neural activity. However, these
 low-level sensory signals, and the neural activity they are represented as, ~~are can be~~ ambiguous with
 respect to the state of the world: for example, the same retinal velocities can correspond to vastly
 different physical velocities, depending on the distance between observer and object. An object that
moves 6 m in front of the observer in the fronto-parallel plane with a physical speed of 1 m/s elicits a
retinal speed of about 9.5°/s when fixation is maintained. The same retinal speed could correspond to a
target that moves at a physical speed of 1.2 m/s 7 m in front of the observer. Decoding, ~~then,~~ is the
 process of interpreting optic flow information. In Decoding, humans often combine sensory input with
 previous (prior) knowledge to obtain a more accurate and precise estimate of the observed state of the
 world. For example, we use knowledge about the size of an object to recover its most likely distance to
 the observer, thus providing a key to recover its physical velocity from retinal motion. If we, for example
know that we are observing a basketball and know from experience that its radius is 0.12 m, and we
perceive that the target occupies a visual angle of 0.5°, we know that the target moves at 7 m in front of
as. We then also know that the physical velocity of the ball is 1.2 m/s, not 1 m/s. In some, if not many
 instances, this combination occurs according to Bayes' formula:

$$P(A|B) = \frac{P(B|A)P(A)}{P(B)} \quad [1]$$

68 The probability of a state of the world A given evidence B is the probability of observing evidence B given
69 the state of the world A multiplied by the probability of the state of the world (A), divided by the
70 probability of the evidence (B). In a Bayesian framework, sensory input (Likelihood), corresponding to the
71 term $\frac{P(B|A)}{P(B)}$ in Equation 1, and prior knowledge (Prior), corresponding to $P(A)$ in Equation 1, are
72 combined according to their respective precisions to yield a more precise and more accurate final percept
73 (Posterior). Under many circumstances, -Prior, Likelihood and Posterior can be represented as normal
74 distributions whose standard deviations correspond to the representation's reliability. If an organism has
75 a high sensitivity to the sensory input, that is, when they are able to reliably distinguish one stimulus
76 strength from a very similar stimulus strength, the standard deviation of the Likelihood would be very low,
77 which corresponds to a very narrow distribution. On the other hand, if the organism has a very precise
78 representation of the most likely state of the world, the Prior would be very narrow. Finally, the standard
79 deviation of the Posterior would depend on the precision of Likelihood and Prior. Usually, both the Prior
80 and the Likelihood contribute to the Posterior; for example when we know that our opponent in a tennis
81 match *usually* serves in the right corner of the court, but *not always*, (Prior) and we have good visibility of
82 their serving motion, but since the motion is so quick, we do not have a lot of time to acquire evidence
83 (Likelihood). We thus take sensory input (e. g. about their body posture while serving) into account only
84 to some extent (see "Normal Prior" scenario in [Figure 1](#)~~Figure-1~~). However, in the case of gravity it seems
85 that the expectation of Earth Gravity overrules all sensory information that humans collect on the law of
86 motion of an observed object (La Scaleia, Zago, & Lacquaniti, 2015; McIntyre et al., 2001; McIntyre, Zago,
87 Berthoz, & Lacquaniti, 2003; Zago & Lacquaniti, 2005b; Zago et al., 2008). On a theoretical level, this is a
88 sensible assumption, since all of human evolution and each human's individual development occurred
89 under Earth Gravity. In Bayesian terms, the Prior is extremely precise and thus overrules all sensory

information represented as the Likelihood. According to our interpretation, we would thus expect an extremely low value for the standard deviation of the earth gravity prior (“Strong Prior” scenario in [Figure 1](#)). We would expect this value to be represented more precisely than linear velocities, which generally elicit Weber Fractions of 10%, which corresponds to a standard deviation of about 15% of the mean represented stimulation.

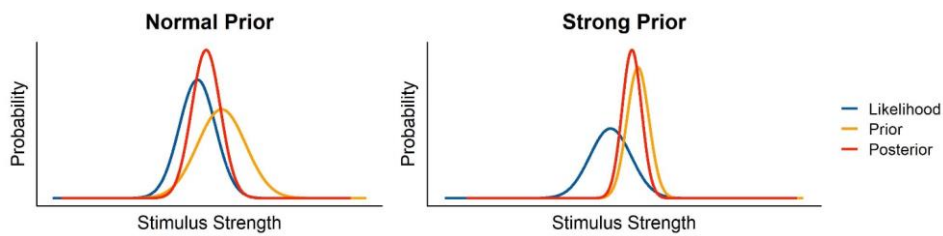


Figure 1: Graphical illustration of Likelihood, Prior and Posterior in a Bayesian framework, for both a normal, relatively shallow Prior, and a strong, extremely precise Prior.

In the following, we use the data from our previous study (Jörges & López-Moliner, 2019) to simulate the variability of responses under different assumptions about the standard deviation of the gravity prior.

Methods

In this paper, we use previously published data (Jörges & López-Moliner, 2019). The pre-registration for the original hypotheses can view viewed on Open Science Foundation (<https://osf.io/8vg95/>). All data relevant to this project are available in our GitHub repository (<https://github.com/b-jorges/SD-of-Gravity-Prior>). We will thus only briefly repeat the most important experimental parameters. We showed participants tennis balls moving on parabolic trajectories in the fronto-parallel plane. The balls could have one out of 6 gravity levels (-1g, 0.7g-1.3g), one out of two initial vertical velocities and one out of two

Field Code Changed

initial horizontal velocities. In trials with a positive gravity value (i.e., downwards acceleration), the target started with an upwards initial velocity component and vice-versa. The target disappeared early after peak (Long Occlusion) or late after peak (Short Occlusion). Each combination of parameters was presented 24 times for a total of 1344 trials. Participants indicated by mouse click when they thought the target returned to its initial height. The stimulus was presented in an immersive 3D environment. Figure 2 provides a 2D illustration of visual scene and target trajectories.

Participants

A total of ten ($n = 10$) participants performed the task, among which one of the authors (BJ). All had normal or corrected-to-normal vision. The remaining participants were in an age range of 23 and 34 years, of which three ($n = 3$) self-identified as women and seven ($n = 7$) self-identified as men. All participants gave their informed consent. The research in this study was part of an ongoing research program that has been approved by the local ethics committee of the University of Barcelona. The experiment was conducted in accordance with the Code of Ethics of the World Medical Association (Declaration of Helsinki).

Stimuli

We presented participants with targets of tennis ball size (radius = 0.033 m), shape and texture that moved on parabolic trajectories. The trajectories were determined by the gravity levels (0.7, 0.85, 1, 1.15, 1.3g, 1g), the initial vertical velocities (4.5 and 6 m/s) and the initial horizontal velocities (3 and 4 m/s). The different kinetic profiles, as well as the occlusion condition (Short Occlusion: last 20-25%; Long Occlusion: last 45-50% of the trajectory), were presented in random order, but the method guaranteed that each combination was presented the same amount of times. The parabolas were presented in the fronto-parallel plane with no change in depth. Air resistance was simulated to provide a

more realistic stimulus. The following equations (<http://www.demonstrations.wolfram.com/ProjectileWithAirDrag/>) determine the x position of the target in time $x(t)$, and the y position of the target in time $y(t)$, respectively, including air resistance:

$$x(t) = \frac{(v_{xt}^2 + v_{yt}^2)^{0.5} + m + g}{g + c} \cos\left(\arcsin\left(\frac{v_{yt}}{(v_{xt}^2 + v_{yt}^2)^{0.5}}\right)\right) + \left(1 - e^{\left(\frac{g+t+c}{m+g}\right)}\right) \quad [2]$$

$$y(t) = \left(\frac{m}{c}\right) + \left((v_{xt}^2 + v_{yt}^2)^{0.5} \sin\left(\arcsin\left(\frac{v_{yt}}{(v_{xt}^2 + v_{yt}^2)^{0.5}}\right)\right) + \frac{m+g}{c}\right) + \left(1 - e^{\left(\frac{g+t+c}{m+g}\right)}\right) \frac{m+g+t}{c} \quad [3]$$

With v_{xt} being the initial horizontal velocity, v_{yt} the initial vertical velocity, m the mass of the target (0.057 kg), g the respective gravity value and c being the drag coefficient, where we chose 0.005.

For description of the parabolas, we use a coordinate system where the observer's position is defined as $x = y = z = 0$; the x axis runs from left to right, the y axis from down to up and the z axis away from the observer in depth. The starting y position was half a meter above the ground ($y = 0.5$ m) for positive gravity values (0.7–1.3g) and 3.5 m for negative gravity values (–1g), while the starting x position was moved to the left from the middle of the scene by half of the overall length of the trajectory ($x = \text{length}/2$ m). The target travels to the right, such that the peak of the parabola was always reached at $x = 0$ m (or the lowest point for the inverted parabolas). The ball's z position remained constant at $z = -6.15$ m. The target disappeared at a random point between 20% and 25% (Short Occlusion) or 45% and 50% (Long Occlusion) of the time it would take for it to return to the initial height ($y = 0.5$ m or $y = 3.5$ m, respectively). The y end position was marked with an elongated table that was displayed in the target area of the room for targets with positive gravities; it was marked with an elongated lamp hanging from the ceiling for inverted stimuli. We presented the trajectories in a rich environment that provided 3D cues about the object's position in depth (see Figure 1) and used a known object (a tennis ball) as target to recruit prior knowledge consistent with the geometry on display. This has been shown to help activate the internal model of gravity (Lacquaniti et al., 2013; Monache, Lacquaniti, & Bosco, 2019; Zago et al., 2011), that we have previously suggested to be an earth gravity prior (Jörges & López Moliner, 2017). This environment was

constructed such that no low-level cues such as differences in brightness and contrast with the target differed significantly between the different trajectories.

Apparatus

Two Sony laser projectors (VPL-FHZ57) were used to provide overlaid images on a back-projection screen

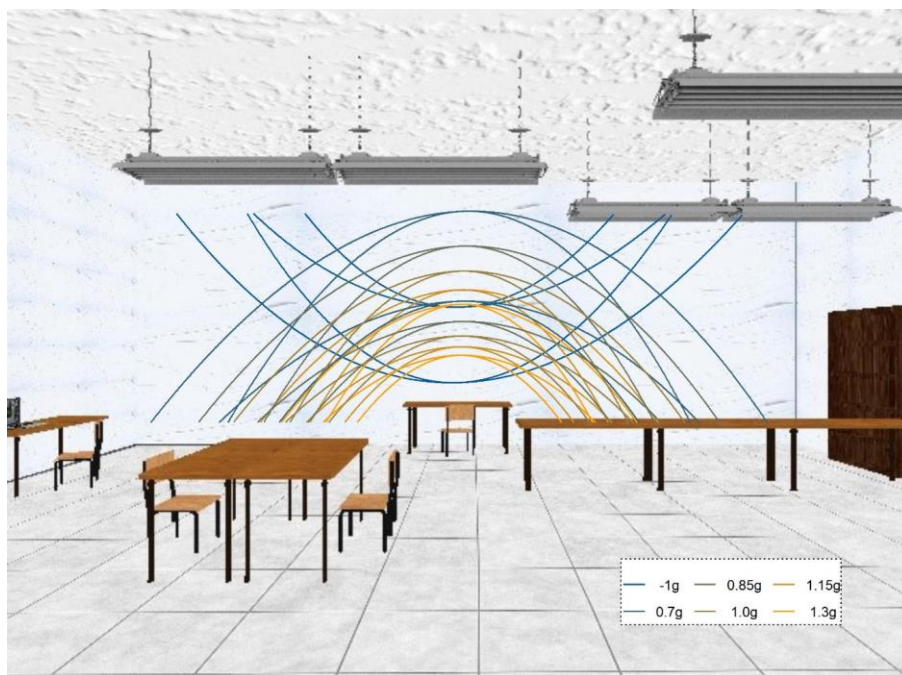


Figure 2: 2D depiction of the visual scene used as environment for stimulus presentation. The stimulus was always presented in front of the white wall and never crossed other areas (such as the lamps of tables) that could introduce low level differences in contrast etc. The lines denote the different parabolic trajectories that along which the targets travelled. [Figure from \(Jörres & López-Moliner 2019\)](#).

(244 cm height and 184 cm width) with a resolution of 1920x1080 pixels. The frequency of refresh of the image was 85 Hz for each eye. Circular polarizing filters were used to provide stereoscopic images. Participants stood at 2 m distance centrally in front of the screen and used polarized glasses to achieve stereoscopic vision of the visual scene and the target. The shown disparity was adapted to each

participant's inter-ocular distance. The stimuli were programmed in PsychoPy (Peirce, 2007); we added the code to our pre-registration (<https://osf.io/8vg95/>). The projectors introduced a delay of 0.049259 s (SD = 0.001894 s) that will be accounted for in the analysis of timing responses. Data was acquired for a different hypothesis, for which we also tracked participants eye movements.

Procedure

Participants were first instructed to pursue the target closely with their eyes and to indicate via mouse button click when they believed the target had returned to the starting level ($y = 0.5$ m/ $y = 3.5$ m). We familiarized subjects with 48 training trials (each combination of experimental variables once), in which the ball reappeared upon mouse click, thus indicating the spatial error. Then, we presented the stimuli in four blocks: 3 blocks of 320 trials each (5 gravities from 0.7g to 1.3g; 2 initial vertical velocities; 2 initial horizontal velocities; 2 occlusion conditions; 8 repetitions per combination). We furthermore tested one block of 1g/1g motion. After each block, participants could take a break. Five subjects (s1, s3, s5, s7, s9) received the 1g/1g block as first block, while the other five subjects (s2, s4, s6, s8, s10) received it as last block.

Results

While we have reported the main results of this experiment in a previous paper (Jörges & López-Moliner, 2019), in the following, we thus limit ourselves to analyzing the influence of gravity on the *precision* of responses in preparation for the simulations we are conducting after, it is worth reiterating the results for the timing task for the conditions we are using in our simulations. We report mean timing errors as well their standard deviations for the 0.7-1.3g trials both

for the Short and the Long Occlusion conditions. We used a slightly different, more liberal outlier analysis for this project to make sure that we don't lose any variability present in participants' responses. Before proceeding to the analysis, we also exclude all data collected from the author (s10; all 1344 trials). Further, we exclude all trials with an absolute error greater than 0.5 s (1091 of 13440 trials). Furthermore, we exclude all trials where subjects pressed the button before the target disappeared (38 trials) or where the temporal error was greater than 2 s (178 trials). Overall, we excluded 1.6% of all trials from the nine participants included in the analysis. (26 of the remaining 12349 trials). Finally, we also excluded subject s09 from these analyses (531 of the remaining 12323 trials) because they displayed a mean temporal error (0.23 s) far above the other subjects (-0.08 to 0.1 s). To make it easier to compare temporal errors across conditions, we then computed the error ratio:

$$\text{Error Ratio} = \frac{\text{Error} + \text{Occluded Duration}}{\text{Occluded Duration}} \quad [4]$$

In Figure 3, we illustrate the response distributions. For an analysis and interpretation of the effect of gravitational motion on accuracy, please see our previous paper (Jörges & López-Moliner, 2019).

To assess biases, we fitted a Linear Mixed Model (using the lme4 package in R) where the Temporal Error is explained by Gravity as fixed effect, and intercepts per Subject as random effects. In lme4 syntax, this translates to:

$$\text{TimingError} \sim \text{Gravity} + (1 | \text{Subject})$$

We compare this Test Model to a Null Model, without fixed effects and only intercepts per Subject as random effects:

$$\text{TimingError} \sim (1 | \text{Subject})$$

An Likelihood Ratio Test showed that the Test Model is significantly better than the Null Model ($p < 0.001$), and the regression coefficient for Gravity is 0.022 (SE = 0.0007). That is, higher gravities are related to higher values of the temporal errors; higher gravities thus lead to too late responses, while lower gravities lead to too early responses. Figure 3 illustrates the distributions of Temporal Errors across subjects.

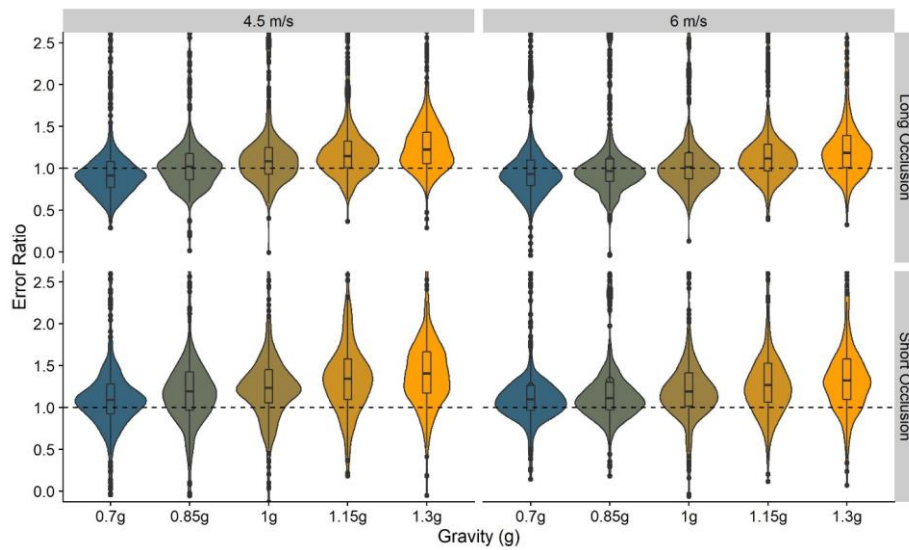


Figure 3: Temporal errors in the 0.7-1.3 g conditions. The wings of each structure indicate the distribution of responses, while the boxplot in the middle of each structure indicate the 75% percentiles and the mean per condition.

While we used Linear Mixed Modelling to assess accuracy, assessing precision differences between conditions is not straight-forward with regular Linear Mixed Modelling this method. Therefore, we employ Bayesian Linear Mixed Modelling to assess whether gravity has an impact on the precision of the timing responses. The R package brms (Bürkner, 2018), which provides user-friendly interface for the package rstan (Stan Development Team, 2016), uses the a very same-similar syntax as to the more well-known lme4 (Bates, Mächler, Bolker, & Walker, 2015). In addition to mean differences, this type of analysis also allows us to test for variability differences between conditions. We thus fit a mixed model to explain both means and standard deviations of the response distributions, with gravity as a fixed effect and varying

intercepts per participant as random effects. Thus, to test whether gravity had an impact on the precision of responses, we established the following test model. In lme4/brms syntax, the test model is specified as:

$Error\ Ratio \sim Gravity + (1 | Subject)$

$Sigma \sim Gravity + (1 | Subject)$

~~$TimingError \sim Gravity + (1 | Subject)$~~

Where the first line corresponds to the statistical structure that corresponds to the means of the response distributions and the second line corresponds to the standard deviations of the response distributions.

Unlike regular Linear Mixed Models, Bayesian Linear Mixed Models do not need to be compared to a Null Model. We can use the hypothesis() function from the R Core package (R Core Team, 2017) to test hypotheses directly. We find a posterior probability of >0.999 of nearly 1 that a higher/lower gravity value is related to lower variability, the sigma value-coefficient for Gravity being -0.0890.057 (SE = 0.004;

		0.7g-1.3 Block					-1g/1g Block	
		Long Occlusion						
v_{yi}		0.7g	0.85g	1g	1.15g	1.3g	-1g	1g
4.5 m/s	Mean	1.12	1.11	1.20	1.24	1.30	1.33	1.17
	SD	0.47	0.49	0.53	0.42	0.44	0.53	0.38
6 m/s	Mean	1.05	1.11	1.17	1.24	1.32	1.23	1.16
	SD	0.49	0.55	0.57	0.54	0.57	0.56	0.46
		Short Occlusion						
v_{yi}		0.7g	0.85g	1g	1.15g	1.3g	-1g	1g
4.5 m/s	Mean	1.22	1.31	1.34	1.41	1.52	1.68	1.35
	SD	0.64	0.65	0.65	0.56	0.88	0.86	0.58
6 m/s	Mean	1.26	1.33	1.37	1.47	1.49	1.51	1.35
	SD	0.65	0.77	0.77	0.88	0.75	0.80	0.76

Table 1: Means and standard deviations observed for the temporal errors divided by gravities and initial vertical velocities.

95% Confidence Interval = [0.051;0.064] in the log space. In the regular space, this corresponds to a standard deviation of 0.296 (95 % CI = [0.282;0.313]) for 0.7g, 0.321 (95% CI = [0.303;0.344]) for 0.85g, 0.350 (95% CI = [0.326;0.378]) for 1g, 0.382 (95% CI = [0.351;0.416]) for 1.15g and 0.413 (95% CI = [0.378;0.458]) for 1.3g. -0.086, 0.072). The reason is most likely that the interval for which the

Commented [BJ1]: We adjusted this table to reflect the changes in dependent variable (ratio instead of absolute error) and outlier analysis

~~motion has to be extrapolated is shorter. Table 1~~ lists all mean temporal errors and the respective standard errors across participants. Note that, unlike the results from the Bayesian Mixed Model, the variability values from also include variability that the Mixed Model assigns to the individual.

~~Table 1: Means and standard deviations observed for the temporal errors divided by gravities and initial vertical velocities.~~

Interestingly, precision seems to be higher for 1g trials than for -1g trials. To test this observation statistically, we fitted a second Bayesian Linear Mixed Model to the -1g/1g data, where gravity as fixed effect factor and subjects as random effects predict the timing error:

$$\text{Error RatioTimingError} \sim \text{Gravity} + (1 | \text{Subject})$$

We tested the hypothesis that Gravity would lead to lower variability. The posterior probability of this hypothesis being true was ~~nearly 1~~ > 0.999, with a sigma ~~value~~ coefficient for Gravity of -0.01109 (SE = 0.004; ~~CI~~ 95 % Confidence Interval = [-0.0142, -0.0096] in the log space. That is, the standard deviation of distribution of -1g responses in regular space is 0.426 (95% Confidence Interval = [0.414;0.439]), while the standard deviation of the distribution of 1g responses in regular space is 0.344 (95% Confidence Interval = [0.334;0.353]). -This indicates that the absolute error is lower and thus the precision is higher for 1g than for -1g. On a theoretical level, this is in line with previous findings (Indovina et al., 2005) showing that the internal representation of gravity is not activated when upwards motion is presented, even when the absolute value of acceleration impacting the object is equal to the absolute value of earth gravity (9.81 m/s²). The precision may thus be higher for 1g than for -1g because the internal model of gravity is utilized for 1g, but not for -1g trials.

251

252 Simulations

253 The physical formula for distance from initial velocity and acceleration (Equation 4) is the base for both of
254 our simulation procedures. This reflects the assumption that humans perform the task at hand accurately
255 – under most circumstances. This assumption is supported by our data, which show a high accuracy for
256 the earth gravity conditions.

257 We furthermore neglect the air drag for these simulations and use the equation for linearly accelerated
258 motion as an approximation.

$$d_y = \frac{g}{2} * t^2 + v_y * t \quad [6]$$

$$t_{1/2} = \frac{-v_y \pm \left(v_y^2 - 4 * \frac{g}{2} * d_y \right)^{0.5}}{2 * \frac{g}{2}} \quad [7]$$

259 As evidenced by a comparison between equations (1) and (2) and equations (3) and (4), the computational
260 complexity increases significantly if we want to accommodate air drag, while the gains in accuracy are
261 marginal (0.02 s in the condition with the most extreme differences).

262

263 Mean of the Gravity Prior

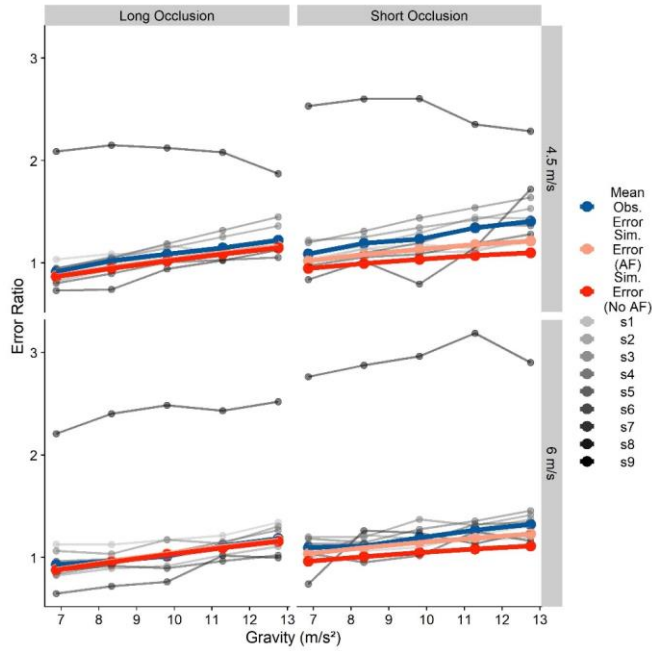
264 To characterize the mean Strong Gravity Prior, we build upon our model the mean timing errors presented
265 in our previous data (Jörges & López-Moliner, 2019). Importantly, the predictions of our model matched
266 the observed data only for the Long Occlusion condition. In the Long Occlusion condition, subjects
267 displayed a tendency to respond slightly too late, while their responses should be centered around zero.
268 Our ad hoc explanation of this discrepancy was that subjects were often executing a saccade when the

269 ball returned to initial height. ~~This saccade which might may~~ have interfered with the predictions. ~~(B-~~
 270 Jörges & López-Moliner, 2019). An alternative explanation may be, however, that our subjects
 271 underestimated the target's speed at disappearance due to the so called Aubert-Fleischl phenomenon:
 272 humans estimate the speed of a target that they pursue with their eyes at about 80% of its actual speed
 273 (Aubert, 1887; de Graaf, Wertheim, & Bles, 1991; Fleischl, 1882; Spering & Montagnini, 2011; Wertheim
 274 & Van Gelder, 1990). Our subjects were specifically instructed to follow the target with their eyes, and the
 275 eye-tracking data we collected that they generally did pursue the target. (Jörges & López-Moliner, 2019).
 276 An underestimation of the velocity at disappearance could explain the tendency of subjects to respond
 277 too late in the Short Occlusion condition. For the Long Occlusion condition, on the contrary, the vertical
 278 speed at disappearance is very low and has a nearly neglectable influence on the final prediction. Setting
 279 the perceived velocity at 80% of the presented velocity should thus yield more accurate predictions for
 280 the Short Occlusion condition, while the accuracy for the Long Occlusion condition would be largely
 281 maintained. We thus employ the same procedure laid out in (Jörges & López-Moliner, 2019), but add a
 282 coefficient of 0.8 to the perceived velocity at disappearance to account for the Aubert-Fleischl
 283 phenomenon.
 284 We will briefly summarize the procedure and then present how this tweak affects the results of our
 285 simulations. We used the physical formula for distance from accelerated motion (Equation 4, with d being
 286 the height at disappearance, v_y the vertical velocity at disappearance and g being gravity). For our
 287 simulations, we assume that humans use an earth gravity value of 9.81 m/s^2 independently of the
 288 presented gravity value, as long as the display is roughly in line with a real-world scenario. We furthermore
 289 assume that we perceive the vertical velocity at disappearance at 80% of the presented velocity. Equation
 290 ~~75~~ thus becomes

$$t_{1/2} = \frac{-v_{y,perceived} \pm \left(v_{y,perceived}^2 - 4 * \frac{g_{earth}}{2} * d_y \right)^{0.5}}{2 * \frac{g_{earth}}{2}} \quad [86]$$

291 With $v_{y,perceived} = 0.8 * v_{y,presented}$ and $g_{earth} = \frac{9.81 m}{s^2}$.

292 We use this formula to simulate the timing error for each trial separately without adding noise. We
 293 furthermore also simulate the responses without accounting for the Aubert-Fleischl phenomenon to
 294 compare performance for both models. ~~Figure 4~~Figure 4 shows the mean errors observed in our
 295 participants ("Obs. Error"), the mean errors when accounting for the Aubert-Fleischl phenomenon ("Sim.
 296 Error (AF)"), and the mean errors when not accounting for the Aubert-Fleischl phenomenon ("Sim. Error
 297 (No AF)").



298
 299 Figure 4: Mean temporal errors that we observed in our participants (*across participants in blue, and for each participant*
 300 *separately in shades of grey*), simulated taking the Aubert-Fleischl phenomenon into account (light red) and simulated without

301 taking the phenomenon into account for the different conditions. The right column represents values for the Long Occlusion
 302 condition, while the left column represents the Short Occlusion condition. The upper row shows values for an initial vertical velocity
 303 of 4.5 m/s, while the lower row represents initial vertical velocities of 6 m/s. Note that the standard errors for the observed errors
 304 are so small that all error bars fall well within the area covered by the dots.

305 The overall Root Mean Squared Error between AF model predictions and observed behavior is ~~0.014~~ 0.2,
 306 and for the non-AF model predictions ~~nearly twice as substantially higher~~, at ~~0.0244~~ 0.265s. ~~Table 2~~ Table
 307 2 shows the error for each of the conditions. Including the AF phenomenon thus vastly improves the
 308 model's generalizability. ~~at the cost of a slight reduction in accuracy for the longest occlusion (Long~~
 309 ~~Occlusion and $v_y = 6$ m/s).~~

v_{yi}	Long Occlusion		Short Occlusion	
	AF	No AF	AF	No AF
4.5 m/s	0.150	0.160	0.236	0.333
6 m/s	<u>0.148</u>	<u>0.158</u>	<u>246</u>	<u>0.344</u>

310 *Table 22: Root Mean Squared Errors (RMSEs) between simulated and observed mean errors for simulations including the*
 311 *Aubert-Fleischl phenomenon (AF) and simulations that don't (No AF). Lower values signify a better fit.*

Commented [BJ2]: Adjusted the values after running simulations again with new outlier analysis

312 This improvement upon our previous model lends further support to the idea that the mean of a strong
 313 gravity prior is at or very close to $9.81/s^2$.

314

315 Standard Deviation of the Gravity Prior

316 The second value needed to characterize a normal distribution, which we assume the strong gravity prior
 317 to be represented as, is its standard deviation. There are two different ways to approach this problem:
 318 First, we can simulate the temporal responses of our subjects assuming different standard deviations for
 319 the gravity prior and minimize the difference between the standard deviations of the responses we

observed in our subjects and the model standard deviations. In this case, we would draw the values for v_y , d_y and g_{earth} from distributions with given means and standard deviations, and compute a simulated temporal response from these values. The mean for v_y would be the last observed velocity in y direction, corrected by a factor of 0.8 for the Aubert-Fleischl phenomenon, and the standard deviation can be computed based on Weber fractions for velocity discrimination from the literature. The mean for d_y is the distance in y direction between the point of disappearance and the reference height. The mean for g_{earth} is 9.81 m/s², and we optimize over its standard deviation to match the standard deviation observed in the subjects' temporal responses.

A second approach would be to solve equation (3) for g_{earth} , and then compute its mean and standard deviation analytically based on the means and standard deviations of t , v_y and d_y . For the addition, subtraction and multiplication of two normal distributions, there are analytic solutions to compute mean and standard deviation of the resulting distribution.

$$g_{earth} = \frac{2(d_y - v_y * t)}{t^2} \quad [86]$$

However, as evident from Equation 5, this method requires computing the standard deviation of the quotient of two distributions. To our knowledge, this is not possible in an analytical fashion and would entail simulations by itself. We will thus focus on the simulation approach.

Assumptions

For this approach, we need to make several assumptions. In the following, we will outline each and provide the rationale for the chosen values. Please note that we conduct these simulations in absolute terms (i.e., absolute errors) to mimic the processes more closely, but convert quality metrics (such as model fits) and results into relative terms (i. e., error ratios).

341 **Use of Equation (3)** – In our previous paper, we have shown that predictions based on Equation 3 fit
342 observed temporal errors reasonably well (Jörges & López-Moliner, 2019). This is particularly the case
343 when subjects extrapolated motion for larger time frames in the Long Occlusion condition. The difference
344 in predictions for this equation with regards to Equation (2) is at most 3 ms, and the added computational
345 complexity does not justify the added accuracy, especially since our main concern is precision.

346 v_y – The velocity term in Equation 4 ($v_y * t$) refers to the part of the full distance the target moved
347 because of its initial velocity. Our targets disappeared right after peak, therefore their initial velocity was
348 very low. The velocity term thus contributes less to the full estimate than the gravity term, especially in
349 the Long Occlusion condition (see also [Figure 5Figure-5C](#)). Importantly, the vertical velocity component is
350 not perceived directly. Rather, it has to be recovered from the tangential speed ($v_{tan,perceived}$) and the
351 angle between the tangential speed vector and the vertical speed vector ($\alpha_{perceived}$) by means of the
352 equation:

$$v_{y,perceived} = \cos(\alpha_{perceived}) * v_{tan,perceived} \quad [9]$$

353 Weber fractions for the discrimination of angular velocities reported in the literature are about 10%
354 (Kaiser, 1990). To calculate the standard deviation of the distribution of perceived velocities from the
355 Weber fraction, we have to find that normal distribution where a difference of 10% from its mean leads
356 to a proportion of responses of 25/75%. For a standardized normal distribution with a mean of 1, this is a
357 standard deviation of 0.148. Note that, by using a standardized normal distribution, we assume that
358 Weber fractions are constant across the relevant range of stimulus strengths. [Figure 5Figure-5C](#) shows
359 how predictions vary with varying variability in perceived vertical velocity: The effect is negligible for the
360 Long Occlusion condition, while it increases response variability uniformly across gravities. Further
361 variability is incurred in estimating $\alpha_{perceived}$. Following (Schoups, Vogels, & Orban, 1995), the JND for

orientation discrimination in untrained subjects is around 6° for oblique orientations. This corresponds to a standard deviation of 0.089.

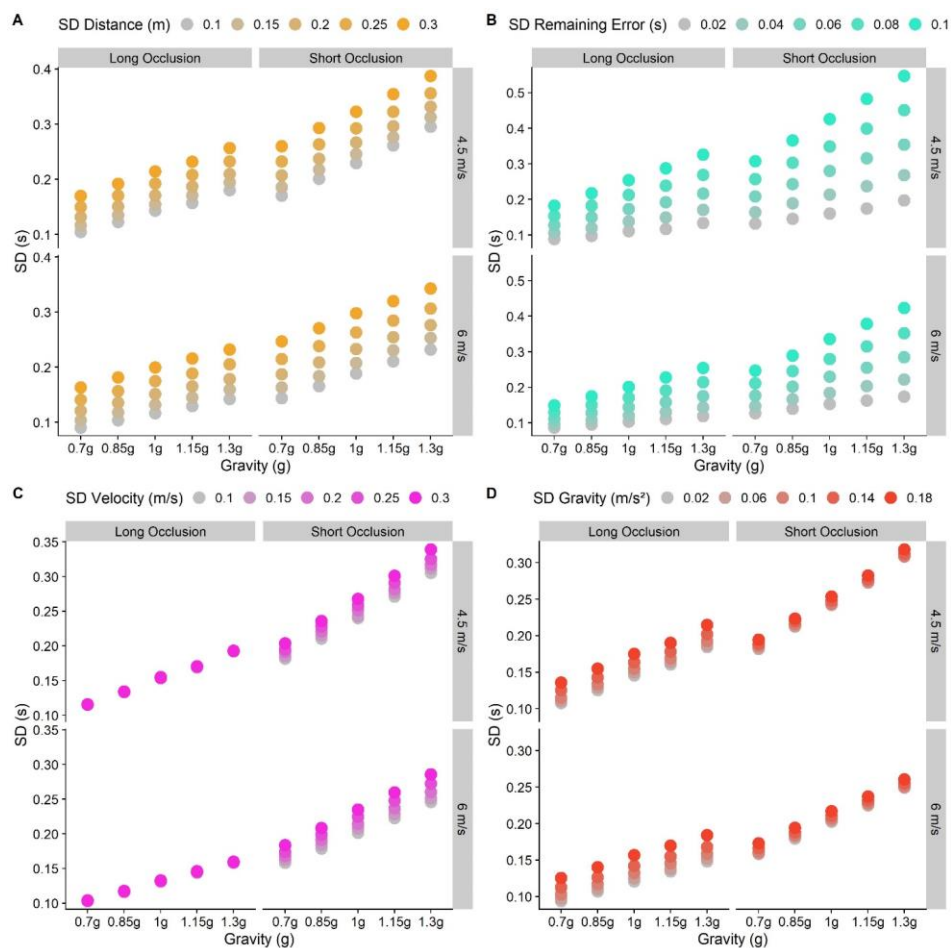
Furthermore, we need to account for the Aubert-Fleischl phenomenon, which consists in an underestimation of the velocity of a moving target during smooth pursuit (Aubert, 1887; de Graaf et al., 1991; Fleischl, 1882; Spering & Montagnini, 2011; Wertheim & Van Gelder, 1990). While this effect should in principle be partially offset by improved predictions for motion coherent with earth gravity – an empirical question that has, to our knowledge, not been addressed so far –, our simulations show that a Aubert-Fleischl correction factor of 0.8 yields an excellent fit for the observed mean errors. We thus proceed with a value of 0.8 also for the simulations concerning the standard deviation.

d_y – For the distance term (d_y), we choose the stimulus value as mean distance, as we don't expect any biases. In terms of precision, Weber fractions of 3% to 5% are observed for distance estimates in the front parallel plane (Norman, Todd, Perotti, & Tittle, 1996). However, since subjects have to estimate the distance not between two well defined points, but rather the height above the simulated table, the precision of these estimates is likely lower than reported for the above task. We thus work with a Weber fraction of twice the reported value (10%). Using the above method, we determine that the standard deviation for this value is 0.148. [Figure 5](#) shows how predictions vary with variability in perceived distance: There is a slight logarithmic pattern, where response variability added by higher variability in perceived distance increases with decreasing gravity.

t – The response time t is measured directly in our task, both in mean and variability.

Remaining Variability – For our simulations, we rely on accounting for every source of variability in the responses. One source of error beyond perceiving and representing g , v_y and d_y is the motor response. Motor responses are likely to vary strongly between tasks, for which reason variability reported in the literature is of limited use. To estimate the error introduced by these further factors, we thus take

385 advantage of previous results indicating that the gravity model is not activated for upside-down motion
386 (Indovina et al., 2005), a hypothesis which is also supported by our data.



387
388 *Figure 5: Predictions for different standard deviations chosen for different parameters in our model. Dots represent the standard*
389 *deviation for each gravity (0.7g-1.3g), divided by Occlusion category (Long and Short) and initial vertical velocities (4.5 and 6 m/s).*
390 *The color gradient indicates different values of the (standardized) standard deviation for the perceived distance, the perceived*
391 *velocity, the represented gravity and the remaining error. The baseline values are 0.148 for distance and velocity, 0.1 for gravity*
392 *and 0.05 for the remaining (motor) error. A. Predictions for five standardized standard deviations for the perceived distance (0.1-*
393 *0.3 m). B. Predictions for five standard deviations for the remaining (motor) error (0.02-0.1 s), modelled as independent of and*
394 *constant across initial velocities, gravities and occlusion conditions. C. Predictions for five different standardized standard*

deviations for the last perceived velocity (0.1-0.3 m/s). D. Predictions for five different standardized standard deviations for the represented gravity (0.02-0.18 m/s²).

Under this assumption, we can use the responses for the inverted gravity condition to estimate the errors introduced by motor variability. An inactivation of the gravity prior would mean that the gravity acting upon the object should be represented with the same precision as arbitrary gravities. We previously found Weber fractions of between 13% and beyond 30% for arbitrary gravities (Jörges, Hagenfeld, & López-Moliner, 2018), which is in line with those found for linear accelerations (Werkhoven, Snippe, & Alexander, 1992). We thus proceed with a value of 20%, which corresponds to a normalized standard deviation of 0.295 (see procedure above).

There are further constraints: First, the motor variability should be lower than the overall variabilities observed for the absolute error in each condition (the minimum is just over 0.08 s for the short occlusion condition with 1.3g and an initial vertical velocity of 4.5 m/s). Second, the motor variability should be equal across conditions and be independent of gravity, initial velocity and Occlusion category (see Figure 5Figure-5B).

We put these values for g , v_y and d_y into Equation 4 to stimulate the temporal responses for each trial 1000 times. We minimize the Root Mean Square Errors (RMSE) between the standard deviations of the simulated timing error and the observed timing errors, separately for each combination of gravity, initial vertical velocity, Occlusion condition and participant. We collapsed the error across initial horizontal velocities because results for both values were virtually the same, mostly likely because the horizontal velocity barely influences overall flight duration in the presence of air drag, and not at all in the absence of air drag. After visualizing a relevant range of candidate values for the standard deviation of the remaining errors (see Figure 6Figure-6), we use the `optim()` function implemented in R with a lower bound of 0.01 s and an upper bound of 0.06 s to find the best fit for the observed data. We found the best fit for a standard deviation of 0.05803 s, with an RMSE of 0.0415 s.

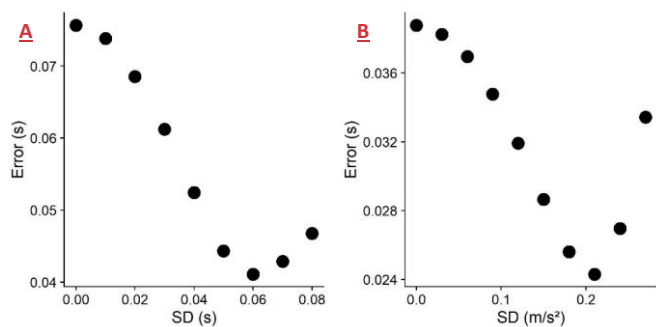


Figure 6: **A.** Root mean square errors (RMSE) between the standard deviation of timing errors simulated based on different motor errors (between 0.00 and 0.07 s) and the standard deviation of observed timing errors. **B.** Root mean square errors (RMSE) between the standard deviation of timing errors simulated based on different standard deviations of the gravity prior between 0.15 and 0.25*9.81 m/s² and the standard deviation of observed timing errors.

Commented [BJ3]: We combined previous Figures 6 and 7 to save space

The Standard Deviation of the Gravity Prior

We then proceed to apply these values to simulate data sets based on the above assumptions, get the standard deviations for the timing error and compare them to standard deviations of the observed timing errors (Method 1). We restrict this comparison to the 0.7g/0.85g/1g/1.15/1.3g condition, as we expect the gravity model not to be activated for inverted gravitational motion. For a discussion of factors impacting the performance of the model for short occlusions, see (Jörges et al., 2018). We first simulate a range of sensible standard deviations (from 0 m/s^2 , corresponding to an impossibly precise representation, to 0.28 m/s^2 , corresponding to a quite imprecise representation with limited impact on the final percept, in steps of 0.03 m/s^2) to determine the lower and upper bounds of the optimization interval (see [Error! Reference source not found. Figure 7](#)); [Figure 5](#) [Figure 5D](#) furthermore highlights how changes in the simulated variability of the represented gravity changes response variability.

We find the errors to be lowest around 0.21 m/s^2 , and choose thus 0.16 m/s^2 as the lower bound and 0.26 m/s^2 as the upper bound. We then search for that standard deviation that minimizes the error

between simulated and observed timing errors, using the `optim()` function implemented in R (R Core Team, 2017). For each iteration, we simulate 1000 data sets and minimize the Root Mean Square Error (RMSE) between the standard deviations of simulated and observed timing errors across these 1000 data sets. The R code we used for these simulations can be found on GitHub (<https://github.com/b-jorges/SD-of-Gravity-Prior>), including extensive annotations. We found a normalized standard deviation of 0.20817 m/s² for the gravity prior, which corresponds to a standard deviation of about 2.0413 m/s² for a mean of 9.81 m/s², and a Weber fraction of 14.16%. The RMSE is 0.02498 s. In Figure 7, we illustrate how the simulated standard deviations relate to the observed ones. The light red dots correspond to this method ("Simulated (Method1)"); as evident from the figure, the fits are better for the short-Long Occlusion condition, while the SDs are generally underestimated/overestimated for the Long/Short Occlusion condition.

Field Code Changed

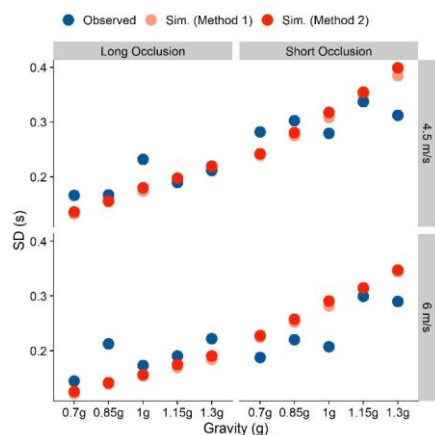


Figure 78: Observed and Simulated Standard Deviations separated by Occlusion Condition, initial vertical velocity and presented gravity. Blue indicates the observed standard deviations across subjects, while the standard deviations simulated through the two-step process (Method 1) are coded light red and the standard deviations simulated through the two-parameter fit (Method 2) are coded solid red.

If the gravity prior was discarded completely for upwards motion, we might observe even larger errors for -1g motion. We elaborate on this issue in the discussion. As there is thus some reason to believe that

457 the gravity prior is not completely inactive in upwards motion, which may bias to above method to
 458 overestimate the standard deviation of the gravity prior, we furthermore conducted simulations where
 459 both the motor variability and the strong gravity prior are fitted to the data (Method 2). To this end, we
 460 use the optimize() function implemented in R which uses the Nelder and Mead method (Nelder & Mead,
 461 1965) to determine those values for the motor standard deviation and the standard deviation of the
 462 gravity prior that yield the smallest errors between simulated and observed variability. This is suitable, ~~as~~
 463 because variability in the gravity prior and motor variability affect the final variability differentially (see
 464 Figure 5~~Figure 5~~): a higher motor variability leads to uniformly higher standard deviations for the observed
 465 error, while a higher gravity variability affects longer trajectories (Long Occlusion, higher initial vertical
 466 velocity and lower gravities) more strongly than shorter ones. Based on above results, we chose 0.04 and
 467 0.2 as starting parameters, but did not limit the parameter space. This method allots variability in slightly
 468 different proportions: the standard deviation for the motor error is 0.065 s and the standardized standard
 469 deviation of the gravity prior is 0.211182 m/s² (which corresponds to a non-standardized standard
 470 deviation of 1.782.07 m/s² and a Weber fraction of 14.2%), with an RMSE of 0.005-024s. ~~This is~~
 471 ~~considerably lower than the RMSE of 0.008 s found with the~~These values are extremely close to the values
 472 found with Method 1. ~~While However, it~~ it is worth noting that fitting both parameters to the data makes
 473 this method more susceptible to overfitting, this lends additional support to the tentative conclusion that
 474 the standard deviation of the gravity prior is just above 2 m/s² or a Weber Fraction of 14.2%. The simulated
 475 standard deviations for these conditions are depicted in solid red in the Figure 8 ("Simulated (Method
 476 2)"): The fits are much better for the long occlusions, at the cost of a slight overestimation of the variability
 477 for the short occlusions.

478

479 Discussion

480 Humans assume in many tasks and circumstances that objects in their environment are affected by earth
481 gravity. It has thus been suggested that we maintain a representation of this value, which we then recruit
482 to predict the behavior of objects in our environment. We recently interpreted this representation as a
483 Strong Prior in a Bayesian framework (Jörges & López-Moliner, 2017). A “Strong Prior” is a prior with a
484 reliability so high that it overrules any sensory input represented in the likelihood. Based on data from
485 timing task (previously reported in Jörges & López-Moliner, 2019), we make an attempt at determining
486 the standard deviation of a hypothetical Strong Earth Gravity Prior. Our general approach is to account
487 for other sources of perceptuo-motor variability in the task based on thresholds reported in the literature,
488 and attributing the remaining variability to the Gravity Prior. Based on this approach, we find a standard
489 deviation of 2.13 m/s² (Method 1) or 2.07 m/s² (Method 2), for a prior with a mean of 9.81 m/s², which
490 corresponds – mathematically – to a Weber fraction of ~~14.6~~14.1% or 14.2%, respectively. This is
491 considerably lower than Weber fractions generally observed for acceleration discrimination, but above
492 Weber fractions for the discrimination of constant speeds (McKee, 1981).

493 Interestingly, when we simulated the timing errors with a fixed value of 9.81 m/s² (i. e. in a non-Bayesian
494 framework where the value of earth gravity is not represented as a distribution, but rather a value set at
495 1g; see Jörges & López-Moliner, 2019 and also above), we found that our results fit the observed timing
496 error quite nicely for each gravity value. That is, the observed gravity (corresponding to the Likelihood)
497 had no discernable influence on the final percept (Posterior). However, in a Bayesian framework, this is
498 only possible if the Likelihood is extremely shallow and the Prior is extremely precise. A Weber fraction of
499 about 30% for the likelihood (which we assume for acceleration discrimination), and a Weber fraction of
500 ~~14.6~~14.1% or 14.2%. for the prior (as modelled) would not result in discarding the likelihood completely
501 (see also Figure 1; even for a strong prior and a rather shallow likelihood, the likelihood attracts the

502 posterior to some extent). Our results thus reveal a mismatch between the means observed in our
503 experiment, the modelled standard deviation and a Bayesian explanation.

504 We see two possible ways to explain this mismatch. Firstly, our observed standard deviation for the gravity
505 prior could be an upper bound. Our method relies on identifying all sources of variability and allotting
506 variability in the response accordingly. Since we did not measure our participants' Weber fractions for
507 velocity and distance discriminations individually, but rather used averages reported in the literature for
508 somewhat different tasks, this may have distorted how much variability perceived distances and velocity
509 at disappearance introduced in the response. Furthermore, when estimating the variability introduced in
510 the motor response, we part from the premise that the internal model of gravity is not activated at all for
511 $-1g$ motion. However, we observe a bias to respond too late in this condition, suggesting that humans
512 expect objects to accelerate less when moving upwards. This could be taken as evidence that the internal
513 model of gravity is still activated to some extent. In this case, we would need to allot more variability to
514 the motor error, which in turn would lead to a lower standard deviation for the gravity prior. However,
515 this pattern in our data is also consistent with humans taking arbitrary accelerations into account
516 insufficiently in perceptuo-motor tasks, which has been reported repeatedly for tasks where the gravity
517 prior is highly unlikely to be recruited (Benguigui, Ripoll, & Broderick, 2003; Bennett & Benguigui, 2013;
518 Brenner et al., 2016; Werkhoven et al., 1992). The values of ~~14.6~~14.1% or 14.2% obtained above may thus
519 be an upper bound for the standard deviation of the Earth Gravity Prior.

520 A second possibility is that prior knowledge and online perceptual input are combined in a non-Bayesian
521 fashion (and we should thus avoid the terminology "Prior", "Likelihood" and "Posterior"), where the mean
522 of the final percept is set according to an acceleration of 9.81 m/s^2 , while its standard deviation is
523 determined by a (not necessarily Bayesian) combination of prior knowledge and online sensory
524 information.

525

526 [Conclusion](#)

527 In this paper, we build upon a simple model for coincidence timing of gravitational motion brought
528 forward in (Jörges & López-Moliner, 2019). By accounting for the Aubert-Fleischl phenomenon, we extend
529 the domain of our model to also include shorter extrapolation intervals. Furthermore, we propose a
530 procedure to determine the standard deviation of a potential gravity prior, and apply it to pre-existing
531 data from a timing task. Standard deviations of 2.13 m/s^2 or 2.07 m/s^2 (depending on the method)
532 explains the behavior observed in our task best. However, considering the literature we would expect an
533 even lower standard deviation, as a Prior with a mean of 9.81 m/s^2 and standard deviations of 2.13 m/s^2
534 or 2.07 m/s^2 should not attract the Posterior as strongly as has been commonly observed. We thus believe
535 that we are not able to fully disentangle different sources of noise in our data; the value we find for the
536 standard deviation of the earth gravity prior is thus more likely an upper bound, and follow-up
537 experiments may find lower values.

538

539 [Author Contributions and Notes](#)

540 BJ conducted the simulations and wrote the paper. BJ and JLM established the research question in a joint
541 effort. JLM provided advice at every step of the project.

542 The authors declare no conflict of interest.

543

544 [Acknowledgments](#)

545 Funding was provided by the Catalan government (2017SGR-48) and the project ref. PSI2017-83493-R
546 from AEI/Feder, UE. The first author (BJ) was supported by the Canadian Space Agency (CSA).

547

548 **References**

- 549 Aubert, H. (1887). Die Bewegungsempfindung. *Pflüger, Archiv Für Die Gesamte Physiologie Des*
550 *Menschen Und Der Thiere*, 40(1), 459–480. <https://doi.org/10.1007/BF01612710>
- 551 Bates, D., Mächler, M., Bolker, B. M., & Walker, S. C. (2015). Fitting linear mixed-effects models using
552 lme4. *Journal of Statistical Software*, 67(1). <https://doi.org/10.18637/jss.v067.i01>
- 553 Benguigui, N., Ripoll, H., & Broderick, M. P. (2003). Time-to-contact estimation of accelerated stimuli is
554 based on first-order information. *Journal of Experimental Psychology. Human Perception and*
555 *Performance*, 29(6), 1083–1101. <https://doi.org/10.1037/0096-1523.29.6.1083>
- 556 Bennett, S. J., & Benguigui, N. (2013). Is Acceleration Used for Ocular Pursuit and Spatial Estimation
557 during Prediction Motion? *PLoS ONE*, 8(5). <https://doi.org/10.1371/journal.pone.0063382>
- 558 Brenner, E., Rodriguez, I. A., Muñoz, V. E., Schootemeijer, S., Mahieu, Y., Veerkamp, K., ... Smeets, J. B. J.
559 (2016). How can people be so good at intercepting accelerating objects if they are so poor at
560 visually judging acceleration? *I-Perception*, 7(1), 1–13. <https://doi.org/10.1177/2041669515624317>
- 561 Bürkner, P. C. (2018). Advanced Bayesian multilevel modeling with the R package brms. *R Journal*, 10(1),
562 395–411. <https://doi.org/10.32614/rj-2018-017>
- 563 Ceccarelli, F., La Scaleia, B., Russo, M., Cesqui, B., Gravano, S., Mezzetti, M., ... Zago, M. (2018). Rolling
564 motion along an incline: Visual sensitivity to the relation between acceleration and slope. *Frontiers*
565 *in Neuroscience*, 12(JUN), 1–22. <https://doi.org/10.3389/fnins.2018.00406>
- 566 de Graaf, B., Wertheim, A. H., & Bles, W. (1991). The Aubert-Fleischl paradox does appear in visually
567 induced self-motion. *Vision Research*, 31(5), 845–849. [https://doi.org/10.1016/0042-](https://doi.org/10.1016/0042-6989(91)90151-T)
568 [6989\(91\)90151-T](https://doi.org/10.1016/0042-6989(91)90151-T)

569 Dichgans, J., Wist, E., Diener, H. C., & Brandt, T. (1975). The Aubert-Fleischl phenomenon: A temporal
 570 frequency effect on perceived velocity in afferent motion perception. *Experimental Brain Research*,
 571 23(5), 529–533. <https://doi.org/10.1007/BF00234920>
 572 Fleischl, V. (1882). Physiologisch-optische Notizen. *Sitzungsberichte Der Akademie Der Wissenschaften*
 573 *Wien*, (3), 7–25.
 574 Gibson, J. J. (1986). *The Ecological Approach to Visual Perception*. New York: Taylor & Francis.
 575 Gold, J. I., & Shadlen, M. N. (2007). *The Neural Basis of Decision Making*.
 576 <https://doi.org/10.1146/annurev.neuro.29.051605.113038>
 577 Indovina, I., Maffei, V., Bosco, G., Zago, M., Macaluso, E., & Lacquaniti, F. (2005). Representation of
 578 visual gravitational motion in the human vestibular cortex. *Science (New York, N.Y.)*, 308(April),
 579 416–419. <https://doi.org/10.1126/science.1107961>
 580 Jörges, B., & López-Moliner, J. (2019). Earth-Gravity Congruent Motion Facilitates Ocular Control for
 581 Pursuit of Parabolic Trajectories. *Scientific Reports*, 9(1). <https://doi.org/10.1038/s41598-019-50512-6>
 582 50512-6
 583 Jörges, Björn, Hagenfeld, L., & López-Moliner, J. (2018). The use of visual cues in gravity judgements on
 584 parabolic motion. *Vision Research*, 149, 47–58. <https://doi.org/10.1016/J.VISRES.2018.06.002>
 585 Jörges, Björn, & López-Moliner, J. (2017). Gravity as a Strong Prior: Implications for Perception and
 586 Action. *Frontiers in Human Neuroscience*, 11(203). <https://doi.org/10.3389/fnhum.2017.00203>
 587 Jörges, Björn, & López-Moliner, J. (2019). Earth-Gravity Congruent Motion Facilitates Ocular Control for
 588 Pursuit of Parabolic Trajectories. *Scientific Reports*, 9(1), 1–13. <https://doi.org/10.1038/s41598-019-50512-6>
 589 019-50512-6

590 Kaiser, M. K. (1990). Angular velocity discrimination. *Perception & Psychophysics*, 47(2), 149–156.
591 <https://doi.org/10.3758/BF03205979>

592 La Scaleia, B., Zago, M., & Lacquaniti, F. (2015). Hand interception of occluded motion in humans: A test
593 of model-based versus on-line control. *Journal of Neurophysiology*, 114, 1577–1592.
594 <https://doi.org/10.1152/jn.00475.2015>

595 La Scaleia, B., Zago, M., Moscatelli, A., Lacquaniti, F., & Viviani, P. (2014). Implied dynamics biases the
596 visual perception of velocity. *PLoS ONE*, 9(3). <https://doi.org/10.1371/journal.pone.0093020>

597 Maffei, V., Indovina, I., Macaluso, E., Ivanenko, Y. P., Orban, G. A., & Lacquaniti, F. (2015). Visual gravity
598 cues in the interpretation of biological movements: Neural correlates in humans. *NeuroImage*,
599 104(October 2014), 221–230. <https://doi.org/10.1016/j.neuroimage.2014.10.006>

600 Marr, D. (1982). A computational investigation into the human representation and processing of visual
601 information.pdf. *Vision: A Computational Investigation into the Human Representation and*
602 *Processing of Visual Information*.

603 McIntyre, J., Zago, M., & Berthoz, A. (2001). Does the Brain Model Newton's Laws. *Nature Neuroscience*,
604 12(17), 109–110. <https://doi.org/10.1097/00001756-200112040-00004>

605 McIntyre, Joseph, Zago, M., Berthoz, A., & Lacquaniti, F. (2003). The Brain as a Predictor: On Catching
606 Flying Balls in Zero-G. In J. C. Buckey & J. L. Homick (Eds.), *The Neurolab Spacelab Mission:*
607 *Neuroscience Research in Space* (pp. 55–61). National Aeronautics and Space Administration,
608 Lyndon B. Johnson Space Center.

609 McKee, S. P. (1981). A local mechanism for differential velocity detection. *Vision Research*, 21(4), 491–
610 500. [https://doi.org/10.1016/0042-6989\(81\)90095-X](https://doi.org/10.1016/0042-6989(81)90095-X)

611 Mijatovic, A., La Scaleia, B., Mercuri, N., Lacquaniti, F., & Zago, M. (2014). Familiar trajectories facilitate

the interpretation of physical forces when intercepting a moving target. *Experimental Brain Research*, 232(12), 3803–3811. <https://doi.org/10.1007/s00221-014-4050-6>

Moscattelli, A., & Lacquaniti, F. (2011). The weight of time: Gravitational force enhances discrimination of visual motion duration. *Journal of Vision*, 11(4), 1–17. <https://doi.org/10.1167/11.4.1>

Nanay, B. (2014). The Representationalism versus Relationalism Debate: Explanatory Contextualism about Perception. *European Journal of Philosophy*, 23(2), 321–336. <https://doi.org/10.1111/ejop.12085>

Nelder, J. A., & Mead, R. (1965). A Simplex Method for Function Minimization. *The Computer Journal*, 7(4), 308–313. <https://doi.org/10.1093/comjnl/7.4.308>

Norman, J. F., Todd, J. T., Perotti, V. J., & Tittle, J. S. (1996). The Visual Perception of Three-Dimensional Length. *Journal of Experimental Psychology: Human Perception and Performance*, 22(1), 173–186. <https://doi.org/10.1037/0096-1523.22.1.173>

R Core Team. (2017). *A Language and Environment for Statistical Computing*. R Foundation for Statistical Computing. Retrieved from <http://www.r-project.org/>.

Schneidman, E., Bialek, W., & Li, M. J. B. (2003). *Synergy, Redundancy, and Independence in Population Codes*. 23(37), 11539–11553.

Schoups, A. A., Vogels, R., & Orban, G. A. (1995). Human perceptual learning in identifying the oblique orientation: retinotopy, orientation specificity and monocularly. *The Journal of Physiology*, 483(3), 797–810. <https://doi.org/10.1113/jphysiol.1995.sp020623>

Senot, P., Zago, M., Le Seac'h, a., Zaoui, M., Berthoz, a., Lacquaniti, F., & McIntyre, J. (2012). When Up Is Down in Og: How Gravity Sensing Affects the Timing of Interceptive Actions. *Journal of Neuroscience*, 32(6), 1969–1973. <https://doi.org/10.1523/JNEUROSCI.3886-11.2012>

634 Spering, M., & Montagnini, A. (2011). Do we track what we see? Common versus independent
635 processing for motion perception and smooth pursuit eye movements: A review. *Vision Research*,
636 51(8), 836–852. <https://doi.org/10.1016/j.visres.2010.10.017>

637 Stan Development Team. (2016). *Stan: the R interface to Stan. R package version 2.14.1*. 1–23. Retrieved
638 from <http://mc-stan.org>

639 Werkhoven, P., Snippe, H. P., & Alexander, T. (1992). Visual processing of optic acceleration. *Vision*
640 *Research*, 32(12), 2313–2329. [https://doi.org/10.1016/0042-6989\(92\)90095-Z](https://doi.org/10.1016/0042-6989(92)90095-Z)

641 Wertheim, A. H., & Van Gelder, P. (1990). An acceleration illusion caused by underestimation of stimulus
642 velocity during pursuit eye movements: Aubert-Fleischl revisited. *Perception*, 19(4), 471–482.
643 <https://doi.org/10.1068/p190471>

644 Zago, M., Bosco, G., Maffei, V., Iosa, M., Ivanenko, Y., & Lacquaniti, F. (2004a). Internal Models of Target
645 Motion: Expected Dynamics Overrides Measured Kinematics in Timing Manual Interceptions.
646 *Journal of Neurophysiology*, 91(4), 1620–1634. <https://doi.org/10.1152/jn.00862.2003>

647 Zago, M., Bosco, G., Maffei, V., Iosa, M., Ivanenko, Y. P., & Lacquaniti, F. (2004b). Fast Adaptation of the
648 Internal Model of Gravity for Manual Interceptions: Evidence for Event-Dependent Learning.
649 *Journal of Neurophysiology*, 93(2), 1055–1068. <https://doi.org/10.1152/jn.00833.2004>

650 Zago, M., La Scaleia, B., Miller, W. L., & Lacquaniti, F. (2011). Coherence of structural visual cues and
651 pictorial gravity paves the way for interceptive actions. *Journal of Vision*, 11(10), 1–10.
652 <https://doi.org/10.1167/11.10.13.Introduction>

653 Zago, M., & Lacquaniti, F. (2005a). Cognitive, perceptual and action-oriented representations of falling
654 objects. *Neuropsychologia*, 43(2 SPEC. ISS.), 178–188.
655 <https://doi.org/10.1016/j.neuropsychologia.2004.11.005>

656 Zago, M., & Lacquaniti, F. (2005b). Internal Model of Gravity for Hand Interception: Parametric
657 Adaptation to Zero-Gravity Visual Targets on Earth. *Journal of Neurophysiology*, 94(2), 1346–1357.
658 <https://doi.org/10.1152/jn.00215.2005>

659 Zago, M., McIntyre, J., Senot, P., & Lacquaniti, F. (2008). Internal models and prediction of visual
660 gravitational motion. *Vision Research*, 48(14), 1532–1538.
661 <https://doi.org/10.1016/j.visres.2008.04.005>

662

663